

FLUID-STRUCTURE INTERACTION IN AN ISOLATED NUCLEAR POWER  
PLANT COMPARING LINEAR AND NONLINEAR FLUID MODELS

FLUID-STRUCTURE INTERACTION IN AN ISOLATED NUCLEAR POWER  
PLANT COMPARING LINEAR AND NONLINEAR FLUID MODELS

By

JOSHUA A. HOEKSTRA, B.Eng (Civil Engineering)

A Thesis Submitted to the School of Graduate Studies in Partial Fulfilment of the  
Requirements for the Degree Master of Applied Science

McMaster University © Copyright by Joshua A. Hoekstra, April 2020

McMaster University MASTER OF APPLIED SCIENCE (2020) Hamilton,  
Ontario (Civil Engineering)

TITLE: Fluid-Structure Interaction in an Isolated Nuclear Power Plant Comparing  
Linear and Nonlinear Fluid Models

Author: Joshua A. Hoekstra

Supervisors: Dr. Michael J. Tait and Dr. Tracy C. Becker

Number of Pages: ix, 46

## ABSTRACT

The long-term operational safety of nuclear power plants is of utmost importance. Seismic isolation has been shown to be effective in reducing the demands on structures in many applications, including nuclear power plants (NPP). Many designs for Generation III+ NPP include a large passive cooling tank as a measure of safety that can be used during power failure. In a large seismic event, the fluid in the tank may be excited, and while the phenomenon of fluid-structure interaction (FSI) has also been studied in the context of base isolated liquid storage tanks, the effect on seismically isolated NPP has not yet been explored. This thesis presents a two-part study on a base isolated NPP with friction pendulum bearings. The first part of the study compares the usage of a linear fluid model to a nonlinear fluid model in determining tank and structural demand parameters. The linear fluid model was found to represent the nonlinear fluid model well for preliminary analysis apart from peak sloshing height, which it consistently underestimated. The second part of the study uses a linear fluid model, an empty tank model and a rigid fluid model to investigate the influence of FSI on the structural response of an isolated NPP compared to a fixed base NPP. In general, the response of a fixed base NPP considering FSI using a linear fluid model can typically be bound by the results assuming an empty tank and assuming a full tank with rigid fluid mass. However, this does not hold for the base isolated NPP, as the peak isolation displacement for an NPP with a linear fluid model at design depth is greater than the peak isolation displacement than the same NPP with an empty tank and with a rigid fluid model.

## ACKNOWLEDGEMENTS

I'd like to thank my friends, here and back home, for believing that I would eventually get to this point and for giving me encouragement during the ups and downs I've had throughout this journey.

I would also like to thank my supervisors for their guidance along the way.

And last, but certainly not least, I would like to thank my family. I wouldn't have been able to make it to this day if not for your constant support and the sound advice you gave me during these times.

# TABLE OF CONTENTS

ABSTRACT .....	iii
ACKNOWLEDGEMENTS .....	iv
TABLE OF FIGURES .....	vi
LIST OF TABLES .....	viii
LIST OF ALL ABBREVIATIONS AND SYMBOLS .....	ix
1. INTRODUCTION .....	1
2. MODEL DESCRIPTION .....	6
2.1 NPP MODEL .....	6
2.2 SEISMIC HAZARD .....	9
2.3 ISOLATION MODEL .....	10
2.4 LINEAR SLOSHING MODEL .....	12
2.5 NONLINEAR SLOSHING MODEL .....	16
3. COMPARISON OF LINEAR AND NONLINEAR FLUID MODEL PERFORMANCE .....	19
4. EFFECT OF FSI ON ISOLATED NPP RESPONSE.....	26
5. CONCLUSIONS.....	36
6. RECOMMENDATIONS FOR FUTURE WORK .....	39
6.1 LUMPED MASS-STICK MODEL .....	39
6.2 ISOLATION MODEL .....	39
6.3 FLUID TANK MODEL .....	40
7. REFERENCES .....	42

## TABLE OF FIGURES

Figure 1. Sample NPP CV (left) and IS (right) stick models. The sticks are joined at the base but are shown beside one another for clarity. ....	7
Figure 2. Elevation view of the concrete CV with passive cooling tank. Dimensions are in m. ....	8
Figure 3. Diablo Canyon and Vogtle UHRS at 10,000-year and 2475-year uniform hazard levels. ....	9
Figure 4. Friction pendulum isolator with the bilinear force-displacement behaviour. ....	12
Figure 5. (a) Cross section of actual tank, (b) cross section of idealized tank, and (c) linear mass-spring model for the tank. ....	13
Figure 6. Mode shapes of sloshing modes (0,1) through (3,4) captured by the nonlinear fluid model (Koh, n.d.). ....	17
Figure 7. Comparison of peak sloshing height of the linear and nonlinear fluid models, for fixed base and base isolated nuclear reactor structures. ....	20
Figure 8. Time history of sloshing heights for Earthquake 5 for the linear and nonlinear fluid models, for fixed base and base isolated nuclear reactor structures. ....	21
Figure 9. Peak tank force with linear and nonlinear fluid models, for fixed base and base isolated NPP. Note the difference in y-axis scales. ....	22
Figure 10. Comparison of mean peak floor acceleration and mean peak displacement for the fixed base and base isolated CV and IS. For the base isolated CV and IS, displacement is shown relative to the isolation system. ....	24
Figure 11. Cross section of sample NPP tank (left) with the idealized equivalent annular tank (right) for the considered fluid depths. ....	27
Figure 12. Comparison of mean peak tank force normalized by tank weight, for varying fluid levels for fixed base and base isolated CV models. ....	28

Figure 13. Mean floor spectra for the fixed base CV with tanks at various fluid depths as a percentage of design depth (DD), at the node where the tank is located. ....	30
Figure 14. Mean floor spectra for the base isolated CV with tanks at various fluid depths as a percentage of design depth (DD), at the node where the tank is located. ....	31
Figure 15. Mean peak floor displacement for the fixed base and base isolated CV models with tanks at various fluid depths. Note the difference in x-axis scales. For the base isolated CV, displacement is relative to the isolation system. ....	32
Figure 16. Mean peak isolation displacements for varying fluid levels. ....	34
Figure 17. Mean peak base shear as a percentage of CV weight for varying fluid levels for fixed base and base isolated CV models. Note the difference in y-axis scales. ....	35



## LIST OF TABLES

Table 1. Containment vessel and internal structure model properties .....	7
Table 2. Water depth variations in tank .....	26

## LIST OF ALL ABBREVIATIONS AND SYMBOLS

<i>CV</i>	= Containment vessel, the protective concrete shell surrounding the reactor
<i>IS</i>	= Internal structure, the frame upon which the reactor and necessary non-structural components are built
<i>NPP</i>	= Nuclear power plant
<i>FSI</i>	= Fluid-structure interaction
<i>UHRS</i>	= Uniform hazard response spectrum
$T_x$	= Fundamental period of $x$
$m_n$	= mass of equivalent mechanical sloshing mode $n$
$c_n$	= damping coefficient of equivalent mechanical sloshing mode $(1, n)$
$k_n$	= stiffness of equivalent mechanical sloshing mode $(1, n)$
$\omega_{1n}$	= natural angular frequency of equivalent mechanical sloshing mode $(1, n)$
$R_o$	= outer radius of annular tank
$R_i$	= inner radius of annular tank
$h$	= fluid depth in tank
$k$	= ratio of inner radius to outer radius
$J_1$	= Bessel Function of the first kind
$Y_1$	= Bessel Function of the second kind
$\xi_{1n}$	= solution to the cross-product of Bessel Functions, used to determine the natural angular frequency of equivalent mechanical sloshing modes
$m_F$	= total fluid mass in tank
$\bar{A}_n$	= an expression used in the derivation for the equation of $m_n$
$C_1(x)$	= cross product of Bessel Functions at point $x$
$m_o$	= rigid mass component of equivalent mechanical fluid model
$T_{x,y}$	= fundamental period of equivalent mechanical sloshing mode $(x, y)$
<i>CFD</i>	= Computational fluid dynamics
<i>SPH</i>	= Smoothed-particle hydrodynamics
<i>LRB</i>	= Lead rubber bearing
<i>DBE</i>	= Design basis earthquake
<i>BDBE</i>	= Beyond design basis earthquake
<i>TSD</i>	= Tuned sloshing damper

# 1. INTRODUCTION

Nuclear power plants (NPP) are critical infrastructure, designed so that the probability of failure is very low in extreme events. A recent, comprehensive study of isolated NPP identified acceptable probabilities of failure for the design of isolated NPP as less than 1% at the design basis earthquake (DBE) level and less than 10% at the beyond design basis earthquake (BDBE) level for nuclear facilities, which corresponds to 10,000-year and 100,000-year shaking hazards, respectively (Kammerer et al., 2019). A common feature of Generation III+ NPP is the incorporation of a large passive cooling tank, located at the top of the structure. During seismic loading, the water in the tank can become excited, and as the mass of water in these passive cooling tanks is often substantial, it may influence the behaviour of the NPP. Previous studies focusing on the Westinghouse AP1000 reactor structure have investigated the influence of sloshing fluid in fixed base NPP on seismic response. Zhao et al. (2014) studied the effects of fluid-structure interaction (FSI) for varying levels of water in the passive cooling tank of an AP1000 reactor building and found that floor acceleration and drift of the structure varied by up to 36% as the water level was altered from empty to design depth. Song et al. (2017) compared the use of a smooth-particle hydrodynamics (SPH) fluid model to an equivalent linear mechanical fluid model as described in Ibrahim (2005) for modelling the fluid in the tank of an AP1000 and found that the equivalent linear mechanical model was in agreement with the SPH model in terms of matching fluid sloshing frequencies and floor response spectra. They also

recommended that FSI be included in seismic analysis of the structure as it can increase floor accelerations in certain period bands by up to 7%. However, in a prior study on the same system also using an SPH model, Xu et al. (2015) found that higher fluid levels could significantly decrease floor accelerations and drifts. Each of these studies used only a single ground motion for analysis. Zhao and Yu (2018) used three ground motions to analyze an AP1000 and found that peak acceleration response of the structure was not necessarily correlated with the fluid volume.

The effectiveness of base isolation in reducing seismic demands on structures is well established for both conventional and nuclear construction. In the context of nuclear construction, isolation not only adds the benefit of reducing seismic demands on the NPP structure and non-structural components but can also reduce costs through the standardization of plant design (Huang et al., 2007). Several studies have illustrated the benefit of isolation on the demand parameters of NPP. Huang et al. (2007) compared the seismic demands to secondary systems of a fixed base NPP to an isolated NPP using several isolation models for high and moderate seismic hazards and found isolation to be effective at consistently reducing demands on secondary systems. Huang et al. (2008, 2010) found that isolation reduced the magnitude of the floor response spectra by approximately 70% compared to a fixed base NPP over the important frequency range of expensive and safety-critical non-structural components as well as reducing floor drift and base shear. Chen et al. (2014) modelled an isolated AP1000 NPP using high-damping

rubber bearings and noted horizontal floor acceleration reductions of 60% compared to the fixed base model. In these studies, fluid-structure interaction was not considered, as no convective fluid action was modelled. Rather, the entire mass of fluid was treated as rigid and included with the mass of the structure. However, reviews of the seismic isolation of NPPs have called for the explicit consideration of FSI in future work (Whittaker et al., 2018).

The combination of isolation and FSI has been studied but less in the context of nuclear facilities. Research on the isolation of both ground- and tower-mounted liquid storage tanks has been conducted. Shrimali and Jangid (2002) subjected both broad and slender ground level base isolated liquid storage tanks to bi-directional excitation and found that the two-component interaction of isolation forces did not influence the seismic response of the tank. It was also observed that sloshing heights were increased when the slender tank was isolated, but isolation was more efficient at reducing tank shear in slender tanks than broad tanks. This is in agreement with findings for an isolated, elevated liquid storage tank investigated by Shrimali and Jangid (2003). Abal and Uckan (2010) found that for a broad tank isolated using friction pendulum (FP) bearings, sloshing heights were not significantly affected when the tank was isolated. Saha et al. (2014) compared several isolation models for ground level water tanks of varying slenderness ratios and found that the main contribution to base shear and overturning moment of the tank was the impulsive mass of fluid. Additionally, isolation models with higher characteristic strength

were found to help limit sloshing displacements. As in Shrimali and Jangid (2002, 2003), isolation was found to increase sloshing heights but also to be more efficient at reducing tank shear in slender tanks than broad tanks. All of these studies modelled the fluid using an equivalent linear mechanical model based on the fluid fundamental sloshing mode. Christovasilis and Whittaker (2008) found that for an isolated ground level tank, an equivalent mechanical fluid model was adequate for representing a finite element fluid model, and that sloshing heights were not significantly affected when the tank was isolated if the isolation and fundamental sloshing periods were well separated. Moslemi and Kianoush (2016) performed a study using a finite element (FE) superstructure and fluid model for an isolated, elevated liquid storage tank and recommended that the isolation period be well separated from the fundamental sloshing period to avoid resonance, which was also recommended by Shrimali and Jangid (2002). While some of these studies have compared linear mechanical fluid models to FE fluid models, none have performed this comparison for an upright annular tank.

Many of the fluid models in these studies are linear and use the fundamental sloshing mode only. The use of nonlinear fluid models is not common when modelling sloshing fluid in an NPP, but nonlinear fluid models have been used when modelling liquid storage tanks and tuned sloshing dampers (TSDs). Love and Tait (2015) showed that for a rectangular tank, an equivalent linear mechanical model provides a good estimate of the resulting lateral tank force compared to a

nonlinear multimodal fluid model but consistently underestimates peak sloshing heights. McNamara et al. (2019) found that a nonlinear, multimodal fluid model for an annular tank was suitable for conducting preliminary TSD design. However, the nonlinear fluid model has not been employed in the analysis of fixed base or base isolated NPPs.

The aim of this study is twofold, 1) to compare the seismic response of an NPP structure with a linear fluid model to a nonlinear fluid model for an annular tank to assess the ability of the linear fluid model to capture key tank and NPP demand parameters, and 2) to investigate the influence of FSI on the seismic response of an isolated NPP. A standard lumped mass stick model is used for the NPP, and a bilinear model is used for the isolation system. Two fluid models are used, a linear equivalent mechanical model and a nonlinear multimodal model, to describe the behaviour of the passive cooling tank. Two locations of existing NPPs in the United States; Diablo Canyon (California) and Vogtle (Georgia), are used in the study. In-plane analysis is conducted using single component ground motions, as the linear equivalent fluid model used is limited to single axis excitation.

## 2. MODEL DESCRIPTION

### 2.1 NPP MODEL

The NPP used in this study is composed of two lumped mass stick models simulated in MATLAB. The models, depicted in Fig. 1, represent the containment vessel (CV), which is the protective shell component of the reactor and the internal structure (IS), which houses the non-structural components of the reactor. The CV and IS share a common base, below which is the isolation system, but are otherwise structurally independent. Mechanical properties for both structures and values for the discrete lumped masses were provided by an industry supplier (A. Saady, 2018). Additional information about the NPP model can be found in Huang et al. (2008) as the model used in this study is similar. Notable differences include the model used in this study being idealized as 2-dimensional, as the analysis was conducted in-plane, whereas the model and analysis in Huang et al. (2008) was 3-dimensional. Moreover, FSI was explicitly considered in this study instead of only modelling the mass of the fluid as rigid.



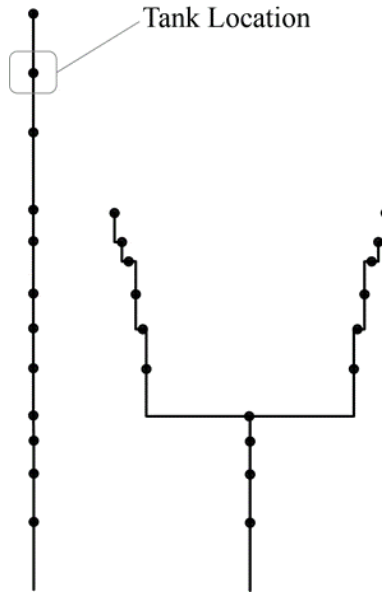


Figure 1. Sample NPP CV (left) and IS (right) stick models. The sticks are joined at the base but are shown beside one another for clarity.

The properties of the CV and the IS are summarized in Table 1. For the CV, the mass at the node of the tank location was altered to account for the mass of the water in the tank, as the original model treated the entire fluid mass of approximately 4300 tonnes as rigid. This represents approximately 17% of the total mass of the CV.

Table 1. Containment vessel and internal structure model properties

	Containment Vessel	Internal Structure
Height (m)	59.5	39
Mass (tonne)	20734 <sup>1</sup> , 25034 <sup>2</sup>	23835
Fundamental Period (s)	0.175 <sup>1</sup> , 0.215 <sup>2</sup>	0.129
Fundamental Period (s) (Huang et al., 2008)	0.2	0.14

<sup>1</sup> Model with empty tank, <sup>2</sup> Model with total fluid mass treated as rigid

The fluid mass was calculated based on the tank size and design depth fill level, Fig. 2. Both the CV and IS are assumed to remain linear elastic during analysis, as would be expected under DBE level ground motions. The fundamental periods of the CV and IS match well with the fundamental period values for the SAP2000 models of the two structures used in Huang et al. (2008). The first and third mode of the CV are lateral, while the second mode is vertical. The periods of the first three modes of the CV with an empty tank are 0.175s, 0.077s, and 0.065s respectively.

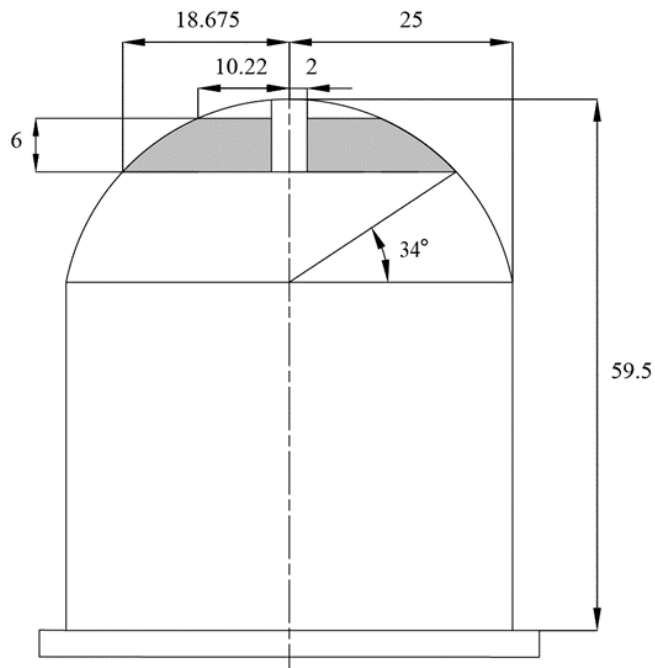


Figure 2. Elevation view of the concrete CV with passive cooling tank.  
Dimensions are in m.

## 2.2 SEISMIC HAZARD

Seismic hazards associated with two sites, Diablo Canyon in California and the lower seismicity Vogtle in Georgia are used in this study. The two sites have been used in previous studies as representative locations for a range of seismic hazards across the United States (Kumar et al., 2017, 2019). The uniform hazard response spectra (UHRS) for the Diablo Canyon and Vogtle sites are shown in Fig. 3. A 10,000-year return period is used in the analysis of safety-critical nuclear facilities (Kammerer et al., 2019); however, to compare the response of the linear and nonlinear fluid tank models, a 2475-year return period is used for the Vogtle site as the nonlinear fluid model can become unstable at high excitation magnitudes.

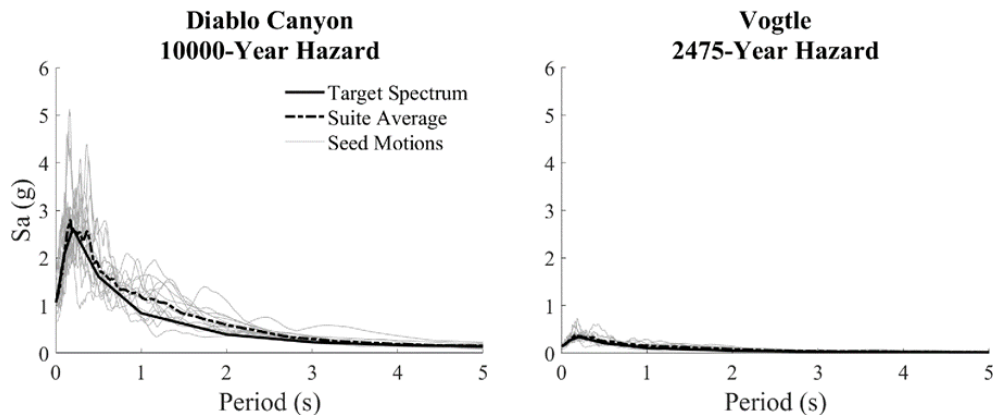


Figure 3. Diablo Canyon and Vogtle UHRS at 10,000-year and 2475-year uniform hazard levels.

Suites of fifteen ground motions were chosen for the Diablo Canyon site and for the Vogtle site as recommended in Kammerer et al. (2019) for presenting mean response values. Ground motions were selected and scaled following NIST (2011)

guidelines. To ensure that motions used in this analysis had optimal spectral shape, magnitude, and site to source distance, they were chosen from suites of ground motions used in prior analyses by Kumar et al. (2019) for the Diablo Canyon and Vogtle NPP sites. The motions were scaled over a period range from  $0.2T_{initial}$  to  $1.5T_{iso}$  (Kumar et al., 2019) where  $T_{initial}$  is the initial stiffness isolation period and  $T_{iso}$  is the second slope period. Since the period range of interest for the isolated NPP model encompasses the period range of interest for the fixed base NPP ( $0.2T_{1,CV}$  to  $1.5T_{1,CV}$ , where  $T_{1,CV}$  is the fundamental period of the containment vessel), the scale factors of the ground motions were kept constant for the analysis of the fixed base and base isolated NPP models. The lists of ground motions used for each site can be found in Appendix A.

### 2.3 ISOLATION MODEL

The isolators used in this study are FP bearings (Fig. 4). FP isolators have been used extensively in conventional construction and are one of the three isolation systems permitted for the seismic isolation of NPP due to their past record of performance and the presence of existing models available that accurately describe their mechanical properties and behaviour (Kammerer et al., 2019). A bilinear model is used to represent the idealized nonlinear behaviour of the FP isolation system. In this study, a single bilinear model is used to represent the entire isolation system,

that is, the weight of the NPP was assumed to be evenly distributed among the isolators, and possible uneven changes in local axial loads were neglected.

The second slope period,  $T_{iso}$ , of a FP isolator is determined by the radius of curvature,  $R$ , and is independent of supported weight:

$$T_{iso} = 2\pi\sqrt{R/g} \quad (1)$$

where  $g$  is the acceleration due to gravity. For the high intensity shaking at the Diablo Canyon site, the isolation system used in this study was designed with a coefficient of friction of 0.02 and radius of curvature of 3.96m, corresponding to a second slope period of 4s. Kammerer et al. (2019) recommended that the isolation system be designed such that its displacement capacity is greater than the 99<sup>th</sup> percentile peak displacement demand for 10,000-year shaking (DBE) and greater than the 90<sup>th</sup> percentile peak displacement demand for 100,000-year shaking (BDBE). Kumar et al. (2019) found that the 90<sup>th</sup> percentile peak displacement demand for 100,000-year shaking was consistently greater than the 99<sup>th</sup> percentile peak displacement demand for 10,000-year shaking and recommended designing the isolation displacement capacity accordingly. As such, the capacity of the FP isolation system used in this study was sized according to the 90<sup>th</sup> percentile peak isolation displacement demand at 100,000-year shaking. The resulting displacement capacity of the isolation system for Diablo Canyon is 1640mm. For the Vogtle site, which is less seismically active, the FP system design has a

coefficient of friction of 0.02 and a radius of curvature of 1.549m, corresponding to an isolation period of 2.5s. The displacement capacity of the Vogtle site isolation system is 470mm.

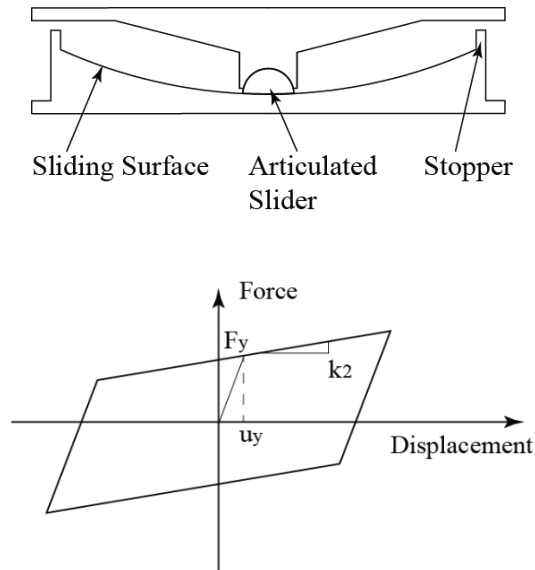


Figure 4. Friction pendulum isolator with the bilinear force-displacement behaviour.

#### 2.4 LINEAR SLOSHING MODEL

The water in the cooling tank is modelled using two methods: 1) a linear equivalent mechanical system and 2) a nonlinear multimodal coupled system, hereafter referred to as linear and nonlinear fluid models, respectively. The linear fluid model assumes that a portion of the fluid moves separately from the tank, termed the convective component, and that the remaining portion of the fluid moves with the tank, termed the impulsive component. The convective component of the fluid

represents the fluid sloshing modes, of which only the asymmetric modes contribute to the net lateral force the fluid produces against the tank wall. Additionally, the fluid response is assumed to remain approximately planar and irrotational (Ibrahim, 2005). The equivalent linear mechanical model, which forms the basis of design code fluid models such as ASCE 4 and Eurocode 8 (Jaiswal et al., 2007), splits the fluid into an impulsive component and a single convective component, which represents the first asymmetric sloshing mode only. In this study, the first four asymmetric sloshing modes are included, as the inclusion of higher sloshing modes is necessary to more accurately predict peak wave height (Svatoslavsky et al., 2013). As shown in Fig. 5c, the rigid fluid mass component,  $m_o$ , is added directly to the lumped mass of the structure at the location of the tank. The four sloshing modes are characterized by  $m_n$ ,  $c_n$ , and  $k_n$  which represent the mass, damping, and stiffness, respectively, of the  $n^{\text{th}}$  sloshing mode.

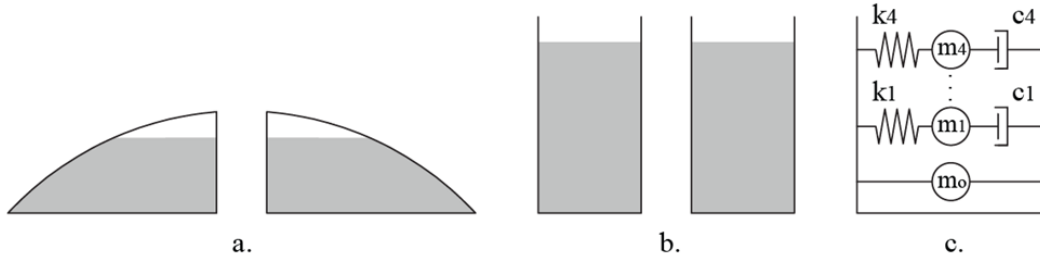


Figure 5. (a) Cross section of actual tank, (b) cross section of idealized tank, and (c) linear mass-spring model for the tank.

The sloshing mode properties depend on the fluid depth and the shape of the tank. For the sample NPP considered in this study, the tank is an upright cylinder with annular cross section and sloped exterior walls, as shown in Fig. 5a. When the tank

is filled to its design depth of 6m, the volume of water is roughly 4300m<sup>3</sup>, with approximately 1m of freeboard. Tanks with irregular geometry are often idealized by creating an equivalent tank of regular geometry with the same volume and surface dimensions. Meserole and Fortini (1987) modelled a toroidal tank using an equivalent annular tank that maintained volume and liquid surface area and found good agreement between the sloshing mode frequencies of the two tanks. Song et al. (2017) modelled an annular tank with a sloped base as an equivalent annular tank with a flat base and found the equivalent tank represented the actual tank well. In this study, the sloped wall annular tank is idealized as an equivalent annular tank. The outer radius and fluid depth were altered to equate the fluid surface area and volume, see Table 2. The idealized tank is shown in Fig. 5b.

The natural angular frequency of the  $(1, n)$  asymmetric sloshing modes in an annular tank is given by Roberts et al. (1966) as

$$\omega_{1n}^2 = \frac{g\xi_{1n}}{R_o} \tanh\left(\frac{h\xi_{1n}}{R_o}\right) \quad (2)$$

In which  $g$  is the acceleration due to gravity,  $R_o$  is the outer radius of the annular tank,  $h$  is the fluid height in the annular tank, and  $\xi_{1n}$  is the  $n^{\text{th}}$  root of Equation 3:

$$J_1'(\xi_{1n})Y_1'(k\xi_{1n}) - J_1'(k\xi_{1n})Y_1'(\xi_{1n}) = 0 \quad (3)$$

where  $k$  is the ratio of inner to outer radius,  $J_1'$  and  $Y_1'$  are Bessel Functions of the first and second kind, respectively, and the prime denotes the derivative with respect to  $\xi_{1n}$ .



The equivalent mechanical masses of the  $(1, n)$  asymmetric sloshing modes as a ratio of the total fluid mass are given by Roberts et al. (1966) as

$$\frac{m_n}{m_F} = \frac{\bar{A}_n \left[ \frac{2}{\pi \xi_{1n}} - k C_1(k \xi_{1n}) \right] \tanh\left(\frac{h \xi_{1n}}{R_o}\right)}{(1 - k^2) \frac{h \xi_{1n}}{R_o}} \quad (4)$$

where  $m_n$  is the mass of asymmetric sloshing mode  $(1, n)$ ,  $m_F$  is the total fluid mass and  $\bar{A}_n$  is

$$\bar{A}_n = 2 \frac{\left[ \frac{2}{\pi \xi_{1n}} - k C_1(k \xi_{1n}) \right]}{\frac{4}{\pi^2} \left( 1 - \frac{1}{\xi_{1n}^2} \right) + C_1(k \xi_{1n})(1 - k^2 \xi_{1n}^2)} \quad (5)$$

In which

$$C_1(k \xi_{1n}) = J_1'(k \xi_{1n}) Y_1'(\xi_{1n}) - J_1'(\xi_{1n}) Y_1'(k \xi_{1n}) \quad (6)$$

For  $j$  convective sloshing modes, the mass of the rigid fluid component can be determined by the following relationship (Ibrahim, 2005):

$$\frac{m_o}{m_F} = 1 - \sum_{n=1}^j \frac{m_n}{m_F} \quad (7)$$

Prior studies that developed expressions for estimating the peak slosh height in a tank using equivalent mechanical models focused on tanks that have rectangular or cylindrical configurations. Bandyopadhyay et al. (1995) presented an expression for wave height for an upright cylindrical tank subject to lateral base shaking only, evaluated in line with the axis of excitation at the outer edge of the tank. Shivakumar et al. (1994) presented the extended solution where wave height can be determined along any radial direction at any distance from the centre of the tank. The number of sloshing modes used in these methods is often limited to one, though

more can be incorporated. This has formed the basis of predicting wave height for the seismic analysis of liquid storage tanks in design codes such as Eurocode 8 and ASCE 4. In these design codes, only the fundamental sloshing mode is considered. Sviatoslavsky et al. (2013) compared wave heights of an annular tank using a computational fluid dynamics (CFD) model to those predicted by an equivalent mechanical model using ASCE 4 and found that the ASCE 4 method underestimated the wave height. However, when the first three sloshing modes were included in the equivalent mechanical model, the wave height was better predicted against the CFD model. As such, here wave height is calculated using the method developed by Shivakumar et al. (1994) considering four sloshing modes.

## 2.5 NONLINEAR SLOSHING MODEL

The nonlinear fluid model used in this study is a coupled multimodal fluid model developed by Faltinsen et al. (2016). Prior work has investigated the suitability of using this type of fluid model for the preliminary design of TSDs (McNamara et al., 2019). As with the linear fluid model, the nonlinear fluid model also represents the sloshing modes by creating a system of equations with respect to the generalized coordinates of the sloshing modes. The model captures weakly nonlinear fluid behaviour through asymptotic relationships between the generalized coordinates of the sloshing modes. Unlike the linear fluid model, the sloshing modes in the nonlinear fluid model are coupled; that is, the response of one sloshing mode

influences the response of the sloshing modes that it is coupled with. In this study, the nonlinear fluid model is composed of 16 sloshing modes; modes (0,1) through (3,4) inclusive. The free surface mode shape of each sloshing mode is displayed in Figure 6.

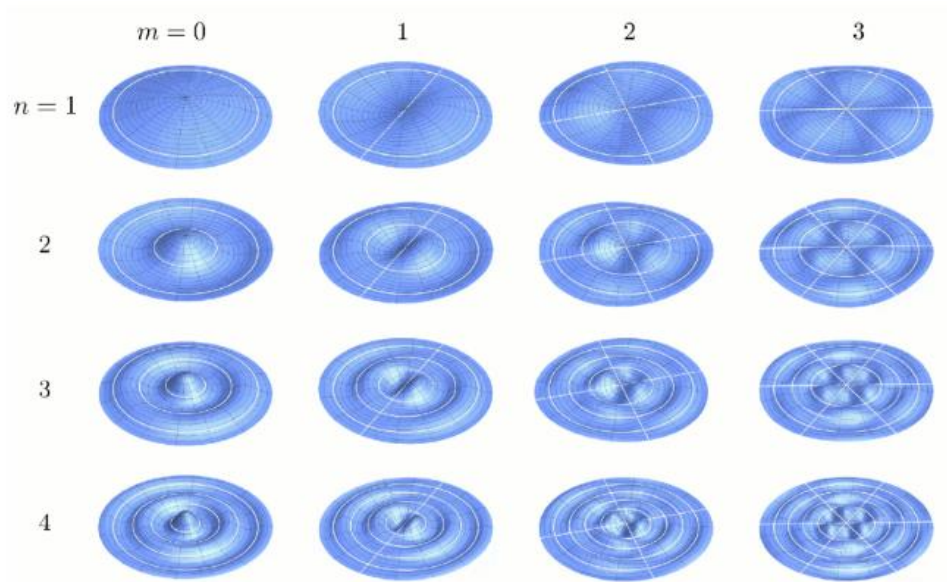


Figure 6. Mode shapes of sloshing modes (0,1) through (3,4) captured by the nonlinear fluid model (Koh, n.d.).

Lateral tank force is calculated using the responses from only the first asymmetric sloshing modes, that is, modes (1,1) to (1,4). These are the same sloshing modes that the linear fluid model uses to calculate tank force. The remaining 12 sloshing modes do not directly contribute to tank force but do contribute indirectly due to modal coupling. Sloshing height is calculated using the responses of all 16 sloshing modes. The nonlinear fluid model is sensitive to excitation magnitude and can become numerically unstable when the excitation amplitude applied to it is too

great, especially when several higher order sloshing modes are included. More information about the nonlinear fluid model can be found in Faltinsen et al. (2016).

### 3. COMPARISON OF LINEAR AND NONLINEAR FLUID MODEL PERFORMANCE

The ability of the linear mechanical model to predict the fluid and structural responses is determined by comparing against the nonlinear fluid model for both fixed base and base isolated cases. Again, ground motions scaled to the 2475-year return period response spectrum for the Vogtle site are used because the numerical stability of the nonlinear fluid model is limited by excitation magnitude. Fig. 7. presents the peak sloshing heights using the linear and nonlinear fluid models, for both the fixed base and base isolated cases of the 2475-year seismic hazard at the Vogtle site. Mean peak sloshing heights for both fluid models are also presented, as presenting a distribution of peak sloshing heights would require results from a set of 30 ground motions instead of 15 (Kammerer et al., 2019).

The peak sloshing heights increase for both the linear and nonlinear fluid models when the NPP is isolated, this is postulated to occur as the average effective isolation period of 1.82s is closer to the fluid sloshing periods than the fundamental fixed base period of the CV (0.175s). As the isolation period approaches the sloshing periods, the floor level input frequency approaches the resonant frequency of the sloshing modes, which results in increased sloshing heights. This is consistent with what has been observed in previous literature for isolated elevated fluid tanks (Shrimali and Jangid, 2002, Seleemah and El-sharkawy, 2011, Moslemi and Kianoush, 2016). Hypothesis testing was not conducted for the mean peak sloshing height for either fluid model.

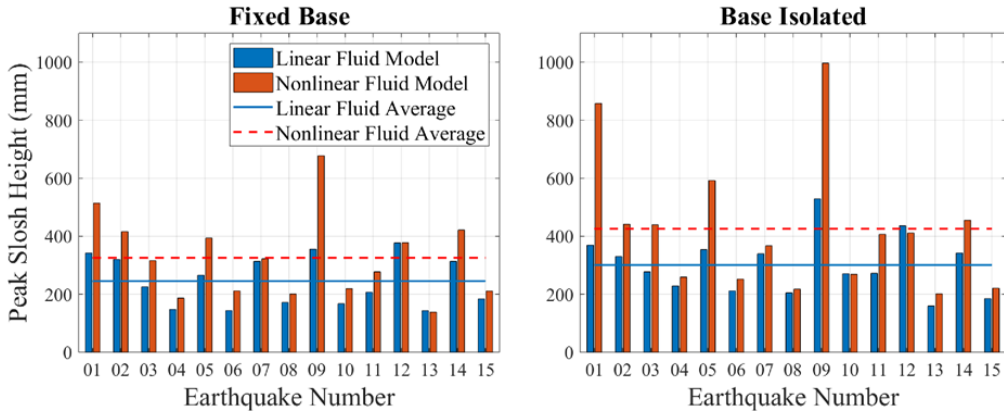


Figure 7. Comparison of peak sloshing height of the linear and nonlinear fluid models, for fixed base and base isolated nuclear reactor structures.

In both the fixed base and base isolated NPP, the nonlinear fluid model predicts higher peak sloshing heights compared to the linear model, however the peak sloshing height of both fluid models remains below the provided freeboard of 1m. The mean peak slosh heights of the nonlinear fluid model are 28.2% and 34.5% higher than the peak slosh heights of the linear fluid model for the fixed base and base isolated structure, respectively. This was also found by Love and Tait (2015) for the fixed base case for a rectangular tank. This is expected as the nonlinear fluid model includes 16 coupled sloshing modes, while the linear fluid model only includes four. Moreover, the nonlinear coupling among the sloshing modes results in a greater excitation of these higher modes. The peak height of these additional sloshing modes can be significant, as observed for earthquake nine for the fixed base NPP and earthquakes one, five, and nine for the isolated NPP. Since the sloshing modes are coupled in the nonlinear fluid model, the drastic response of

one sloshing mode influences the response of the other sloshing modes, further increasing peak sloshing height. This is illustrated in Fig. 8 for earthquake five, where the peak sloshing height of the nonlinear fluid model has a greater relative increase when base isolated than the peak sloshing height of the linear fluid model. These ground motions that substantially excite sloshing modes only included in the nonlinear fluid model account for most of the difference in mean peak slosh height between the two fluid models. Thus, the linear fluid model should not be used to estimate peak slosh height.

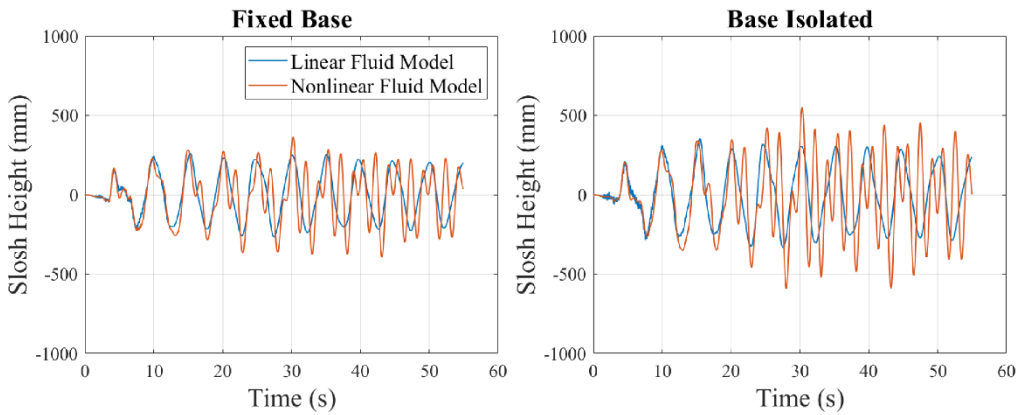


Figure 8. Time history of sloshing heights for Earthquake 5 for the linear and nonlinear fluid models, for fixed base and base isolated nuclear reactor structures.

The peak lateral force of the passive cooling tank for the two fluid models is shown in Fig. 9 for the fixed base and base isolated NPP. When the NPP is isolated, the peak tank force decreases considerably for both the linear and nonlinear fluid models. This was also observed in prior studies when linear (Paolacci, 2015) and finite element (Christovasilis and Whittaker, 2008) fluid models were used in the

analysis of liquid storage tanks. This reduction in tank force when the structure is isolated is primarily associated with the reduction in acceleration of the rigid component of the fluid that moves with the structure. Again, hypothesis testing was not conducted for the mean peak tank force for either fluid model.

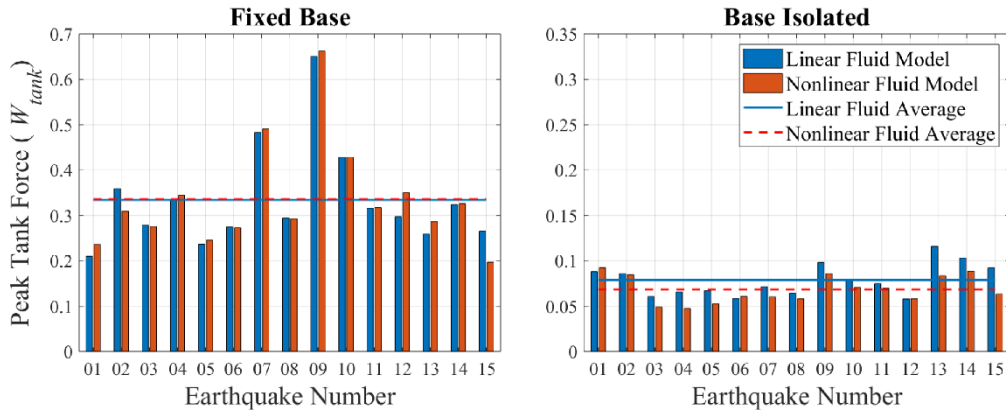


Figure 9. Peak tank force with linear and nonlinear fluid models, for fixed base and base isolated NPP. Note the difference in y-axis scales.

The linear and nonlinear fluid models predict similar peak tank forces. For the fixed base NPP reactor structure, the maximum difference in peak tank force between the nonlinear and linear fluid models is 0.5%. For the isolated NPP, the nonlinear fluid model produces lower peak tank forces by up to 14.2%. The linear fluid model is in better agreement with the nonlinear model when predicting peak tank force (rather than peak sloshing height) as tank force is determined using only asymmetric sloshing modes in the linear model, and only the first asymmetric sloshing modes in the nonlinear model, whereas sloshing height is influenced by both symmetric and asymmetric modes. As the linear fluid model does not include



symmetric sloshing modes, peak tank force can be well represented compared to the nonlinear fluid model when the NPP reactor structure is fixed base and is slightly overestimated by the linear fluid model when the NPP reactor structure is base isolated.

The structural response parameters of the NPP reactor structure are the most important behaviour as they also drive the performance of non-structural components. Fig. 10. shows the mean peak floor displacements and accelerations for each node of the fixed base and base isolated CV and IS for the linear and nonlinear fluid models. The floor acceleration of the CV with the linear fluid model matches the nonlinear fluid model well at each point for both the fixed base and base isolated cases. At the top node of the CV, the difference in mean peak acceleration between the linear and nonlinear fluid model is 0.3% (0.002g) when the CV is fixed base and 13.9% (0.017g) when the CV is base isolated. The mean peak floor acceleration of the base isolated CV with the linear fluid model tank is slightly larger than with the nonlinear fluid model tank, which is consistent with the findings of tank force. This is also true for the IS, where the difference in mean peak acceleration between the linear and nonlinear fluid model at the top node is 11.4% (0.099g) when the CV and IS are isolated. Although the tank is not part of the IS stick model, there is a difference in mean peak acceleration of the IS when isolated because the IS and CV are joined at the base. The change in response of the CV (due to the different fluid models) leads to a change in response of the

isolation system, which affects the IS. The tank does not affect the acceleration of the IS when the CV and IS are fixed base.

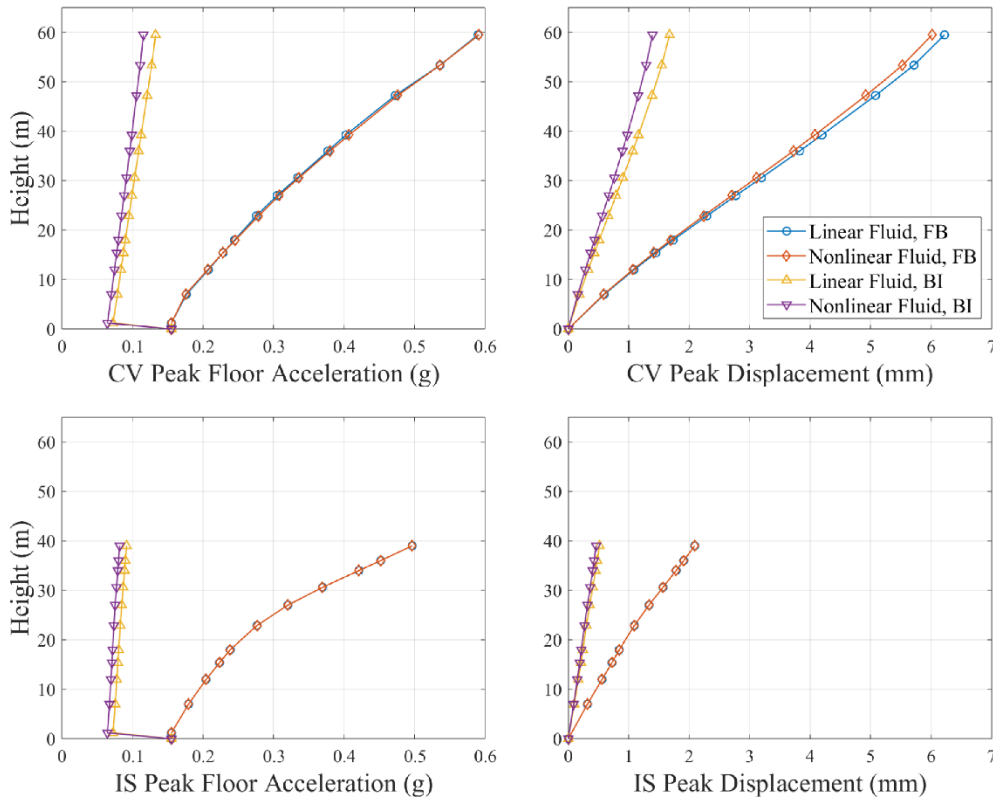


Figure 10. Comparison of mean peak floor acceleration and mean peak displacement for the fixed base and base isolated CV and IS. For the base isolated CV and IS, displacement is shown relative to the isolation system.

Similar conclusions are drawn for the comparison of mean peak floor displacement for the CV with the linear and nonlinear fluid model tanks. The mean peak displacement of the CV with the linear fluid model matches well with the nonlinear fluid model for both fixed base and base isolated cases. At the top node of the CV, the difference in mean peak displacement between the linear and nonlinear fluid

model is 3.4% (0.21mm) when the CV is fixed base and 18.4% (0.28mm) when the CV is base isolated. The base isolated CV with the linear fluid model has slightly larger mean peak floor displacement than the CV with the nonlinear fluid model, which again is consistent with the tank force predictions. This is also true for the IS when the CV and IS are base isolated. At the top node of the IS, the difference in mean peak displacement between the linear and nonlinear fluid model is 11.4% (0.06mm) when isolated. As with the acceleration of the IS, the change in displacement of the IS comes indirectly from the change in response of the isolation system, which itself is caused by the change in response of the CV. The tank does not affect the displacement of the IS when the CV and IS are fixed base.

From the comparisons using linear and nonlinear fluid models to represent the passive cooling tank of the CV, it is demonstrated that predictions of tank force, floor displacement, and floor acceleration are sufficiently close to allow for the use of a linear fluid model for preliminary analysis. Since the sloshing forces of the linear fluid model and nonlinear fluid model were found to be in good agreement, it is also expected that the floor acceleration and displacement be in good agreement. However, wave height can be underestimated when a linear fluid model is used for the tank. A nonlinear fluid model should be used for tank design, including parameters such as the amount of freeboard to provide.

## 4. EFFECT OF FSI ON ISOLATED NPP RESPONSE

As the linear fluid model is suitable for preliminary analysis, the linear fluid model is used to investigate the influence of FSI on the structural responses of a base isolated NPP. As the fluid depth to outer radius ratio of an annular tank decreases, the proportion of fluid that participates in sloshing increases, influencing response. Thus, four fluid depths were considered. Additionally, the tank was modelled as empty to use as a bounding case. Lastly, the tank at design depth was also modelled with all fluid acting rigidly, neglecting FSI, as is often done in studies of NPP (Huang et al., 2008). These cases are outlined in Table 2. For cases 1-4, the outer radius and fluid depth of the idealized annular tank were altered to ensure that liquid surface area and volume matched that of the actual tank at the given fluid height. This is shown in Fig. 11.

Table 2. Water depth variations in tank

Case	Description	Fluid Model	Fluid Depth (m)	Volume (m <sup>3</sup> )	Sloshing Mode (1,1) Period (s)
1	25% of Design Depth	Linear	1.5	1497	15.06
2	50% of Design Depth	Linear	3	2727	9.21
3	75% of Design Depth	Linear	4.5	3667	6.40
4	Design Depth	Linear	6	4300	4.96
5	Tank Empty	Empty	0	0	N/A
6	Rigid Fluid (Design Depth)	Rigid	6	4300	N/A

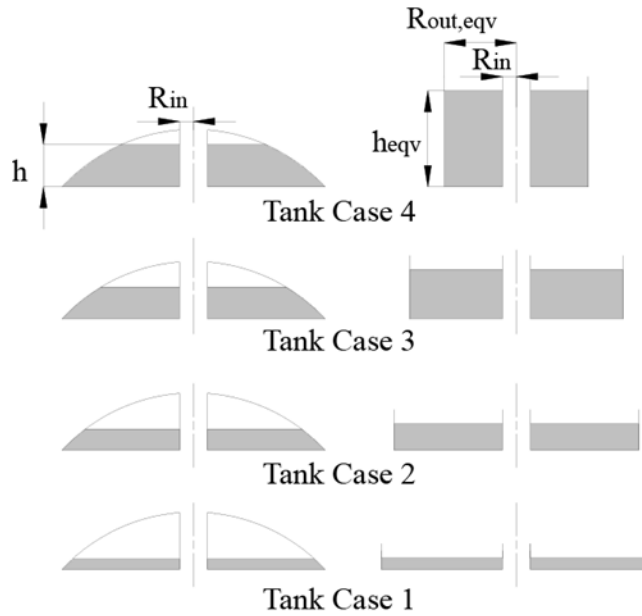


Figure 11. Cross section of sample NPP tank (left) with the idealized equivalent annular tank (right) for the considered fluid depths.

Results for fixed base and base isolated NPP are presented to provide a benchmark for the effects of FSI on the base isolated cases. Fifteen ground motions were scaled to the 10,000-year Diablo Canyon UHRS. Fig. 12. shows the mean peak lateral tank forces normalized by fluid weight as a function of fluid depth. The dashed line displays the tank force for the rigid fluid model, which treats the entire fluid mass as rigid thus omitting any potential fluid sloshing effects. For both the fixed base and base isolated CVs, normalized tank force increases with fluid depth. Since the equivalent annular tank preserves fluid volume and surface area, it becomes more slender as fluid depth increases. As the tank becomes more slender, the proportion of impulsive fluid which is considered as rigidly attached to the CV increases. Since the impulsive fluid is rigidly attached to the CV, it experiences the same high

acceleration demands as the CV, due to the CV's short fundamental period (0.175s). As such, this impulsive fluid component contributes more to the net tank force than the convective fluid component, which experiences lower acceleration demands due to the longer periods of the sloshing modes (see Table 2). For the fixed base CV, the rigid fluid model produces the largest mean peak tank force and acts as an upper bound for the linear fluid model tanks. The rigid fluid model provides a conservative estimate of peak tank force when the CV is fixed base.

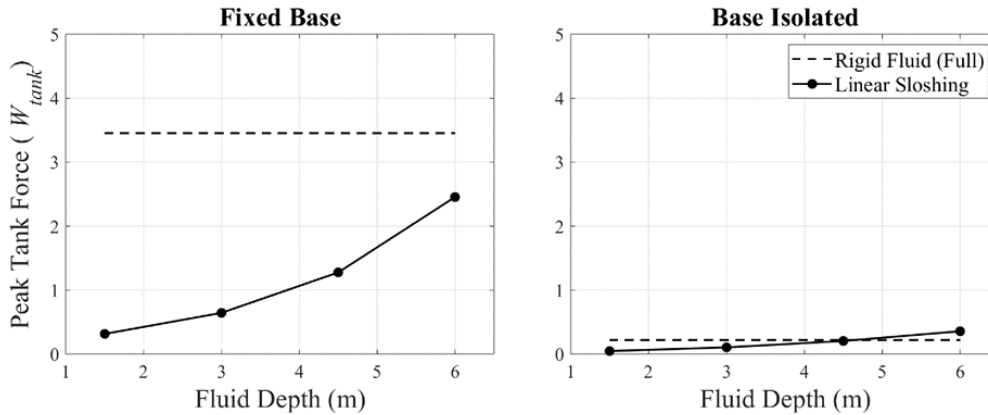


Figure 12. Comparison of mean peak tank force normalized by tank weight, for varying fluid levels for fixed base and base isolated CV models.

For the base isolated NPP, the impulsive fluid component contributes less to the net tank force than when the NPP is fixed base, as the acceleration is significantly decreased due to the isolation layer. Thus, the convective fluid component accounts for a much greater percentage of net tank force. For the isolated CV, the rigid fluid model has lower mean peak tank force than the linear sloshing model with 4.5m and 6m depths. As the tank becomes more slender, the periods of the asymmetric

sloshing modes decrease and begin to approach the average effective isolation period of 3.73s, which causes an increase in response from the convective fluid. For the base isolated CV, the rigid fluid model no longer acts as an upper bound on mean peak tank force, and no longer provides a conservative estimate of peak tank force.

The mean floor response spectra at the tank node of the fixed base CV for each fluid level is shown in Fig. 13. For the fixed base NPP, the highest peak for the floor response spectra occurs at the fundamental period of the CV, which changes slightly from the empty tank CV (0.175s) to the rigid fluid CV (0.215s). As the depth of the linear fluid model increases, the shape of the floor response spectra shifts from the empty tank floor response spectra towards the rigid fluid floor response spectra. This is expected, as increasing the depth of the fluid increases the proportion of fluid modelled as an impulsive mass, which brings the mass and period of the linear fluid CV model closer to those of the rigid fluid CV model. At all fluid depths, the ordinates of the linear fluid CV model floor response spectra are bound by the empty tank and rigid fluid model floor response spectra across the full period range. As a result, it can be inferred that including the effects of FSI will not influence the acceleration values of the floor response spectrum for a fixed base NPP.

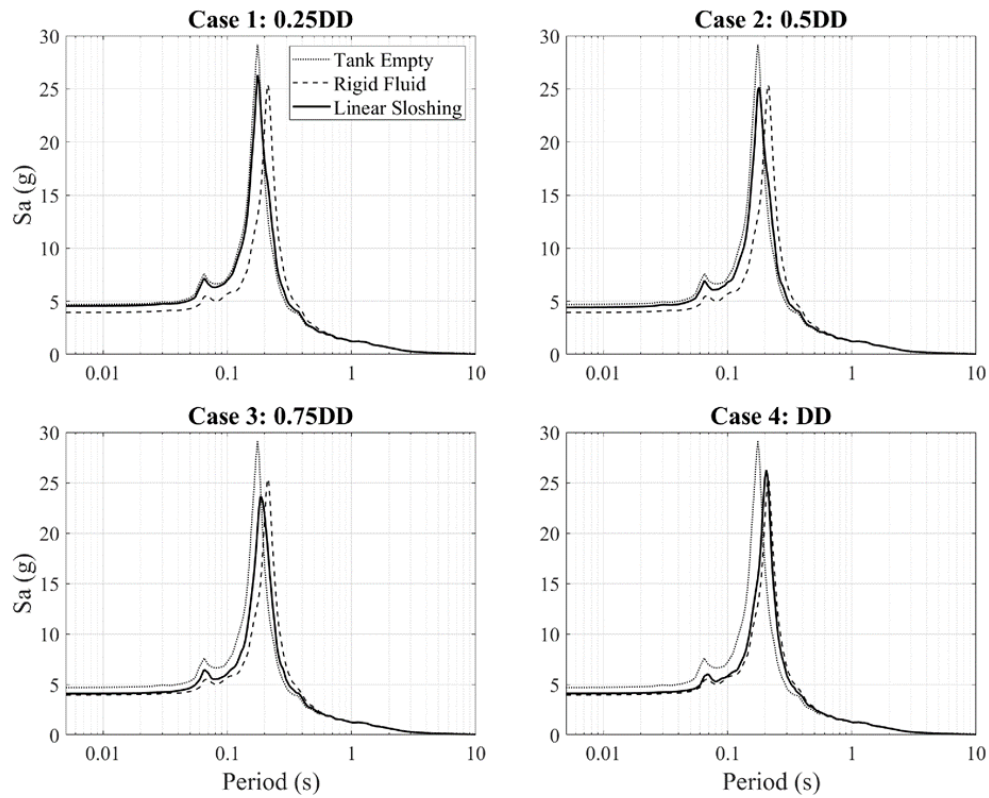


Figure 13. Mean floor spectra for the fixed base CV with tanks at various fluid depths as a percentage of design depth (DD), at the node where the tank is located.

The mean floor response spectra for the tank node of the base isolated CV for each fluid level are shown in Fig. 14. The floor response spectra for the base isolated CV follow the same general trend as for the fixed base CV. As fluid depth increases, the floor response spectra shift in shape and magnitude to more closely resemble the rigid fluid floor response spectra. However, unlike the fixed base cases, the envelope of the empty tank and rigid fluid model floor response spectra curves do not encompass the linear fluid model floor response spectra curves across the full period range. For periods in the 3-5s range, the floor response spectra of the linear



fluid CV model are greater than the ordinates of the rigid fluid and empty tank model floor response spectra. The increase is minor when the tank is 50% and 75% of design depth full but much greater when the tank is filled to its design depth. This can be attributed to the interaction between the isolation and fluid sloshing modes, which is most significant when the tank is filled to design depth.

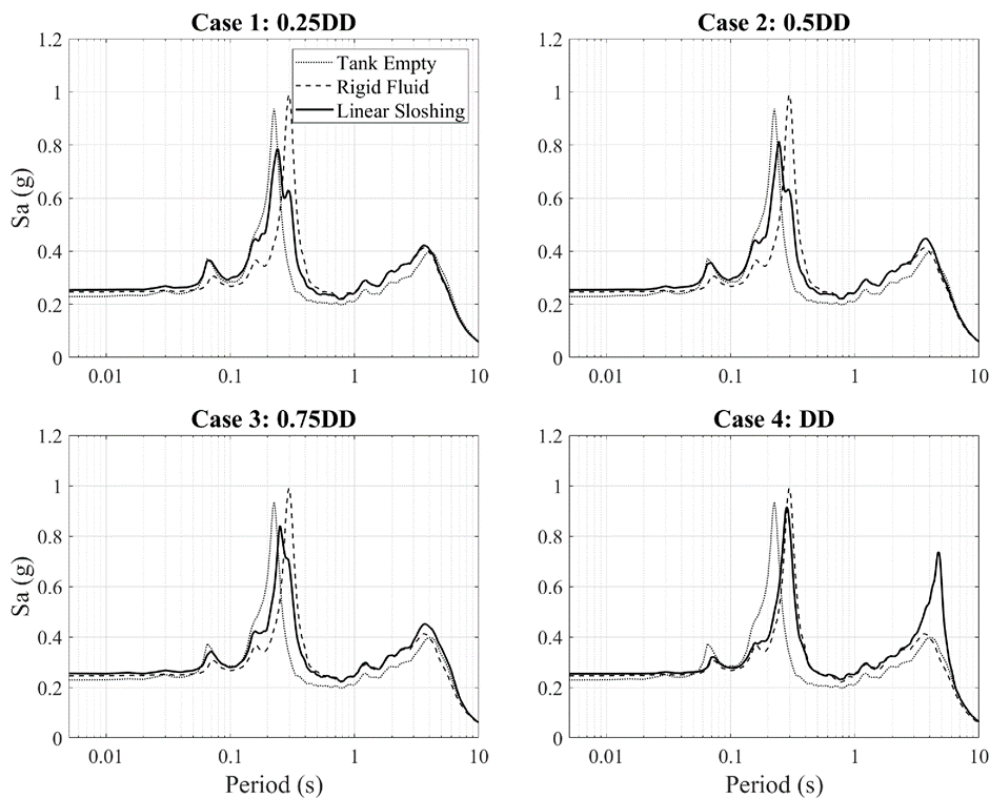


Figure 14. Mean floor spectra for the base isolated CV with tanks at various fluid depths as a percentage of design depth (DD), at the node where the tank is located.

Figure 15 shows the mean peak floor displacement for the fixed base and base isolated NPPs for each fluid model case. For the isolated CV models, mean peak

floor displacement is measured relative to the isolation system so that results can be directly compared with the fixed base CV models. Mean peak floor displacements follow the same patterns for both fixed base and base isolated NPP. When the fluid level increases in depth, the displacement increases. The empty tank and rigid fluid cases act as lower and upper bounds, respectively, on the mean peak displacement of the linear fluid cases. This is analogous to what is observed for mean peak tank force for the fixed base CV model. As the impulsive proportion of fluid increases and moves in phase with the CV, it elongates the fundamental period of the CV, increasing displacement. The same phenomenon is also observed for the base isolated CV model, where the empty tank and rigid fluid models provide lower and upper bounds, respectively, on mean peak displacement relative to the isolation system.

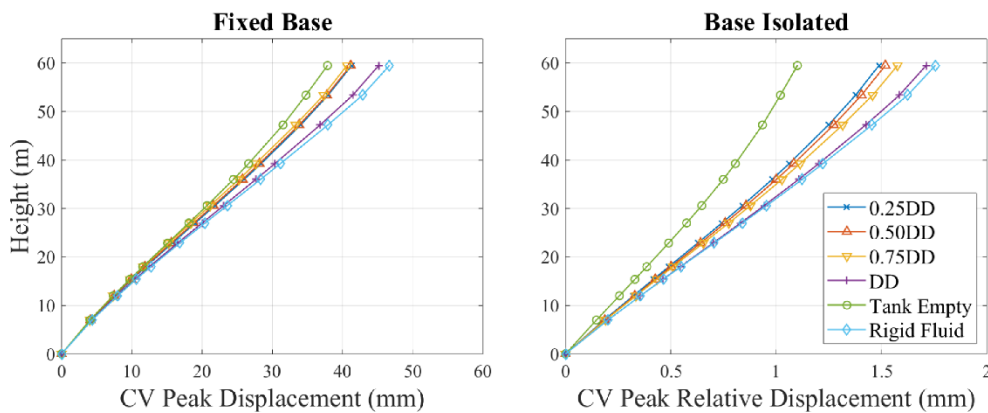


Figure 15. Mean peak floor displacement for the fixed base and base isolated CV models with tanks at various fluid depths. Note the difference in x-axis scales. For the base isolated CV, displacement is relative to the isolation system.

Figure 16 shows the mean peak isolation displacement as a function of fluid depth. The CV with the linear fluid model at the design depth has greater mean peak isolation displacement than the CV with either the empty tank or rigid fluid models, which do not act as lower and upper bounds as they do for mean peak CV displacement. At the design depth, the equivalent annular tank has sloshing periods of 4.96s, 2.88s, 2.21s, and 1.84s for the first four asymmetric sloshing modes, which are close to the average effective isolation period of 3.73s. The increase in isolation displacement can be attributed to the excitation of the asymmetric sloshing modes, especially the first asymmetric sloshing mode, which constitutes most of the convective fluid mass. This modal coupling effect is not captured by the empty tank model or the rigid fluid model. However, this modal coupling effect decreases significantly when the fluid depth drops below 6m. At the depth of 4.5m, the first four asymmetric sloshing modes have periods of 6.40s, 3.26s, 2.53s, and 2.13s respectively. Although the second and third asymmetric sloshing mode periods become closer to the effective isolation period, the fundamental asymmetric sloshing mode period becomes further separated, which decreases the influence of the convective fluid on isolation displacement. Any significant effects of FSI disappear at fill depths of 3m and 1.5m, as at those depths sloshing periods are well separated from the isolation period, and the mass contribution of the second, third and fourth asymmetric sloshing modes is minimal.

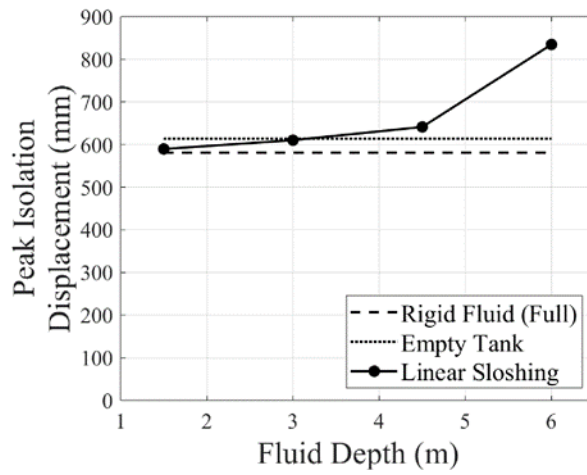


Figure 16. Mean peak isolation displacements for varying fluid levels.

The peak base shear for the fixed base and base isolated NPP is shown in Fig. 17. There is a significant reduction in base shear from the fixed base CV to the base isolated CV, which is expected as the isolation layer effectively elongates the fundamental period of the CV from 0.175s (empty tank case) to 3.73s. This elongation of the fundamental period drastically reduces the acceleration demand to the CV, as illustrated in Fig. 3.

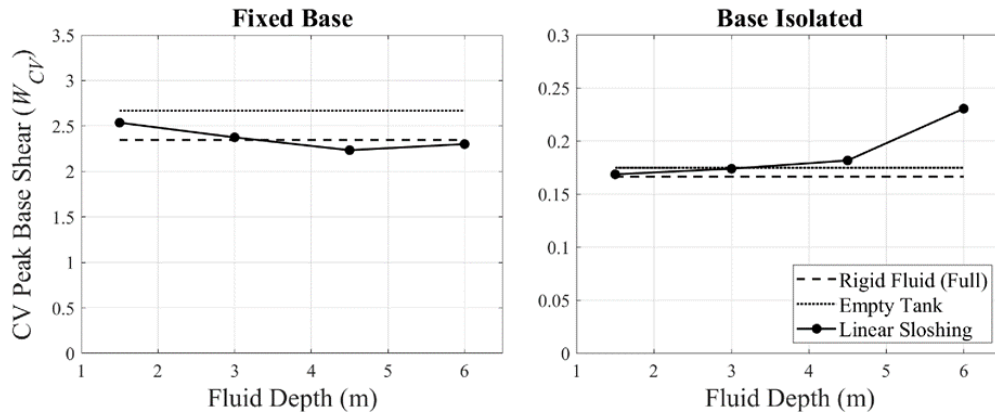


Figure 17. Mean peak base shear as a percentage of CV weight for varying fluid levels for fixed base and base isolated CV models. Note the difference in y-axis scales.

For the fixed base NPP, the empty tank model has the highest mean peak base shear, and the base shear generally decreases as fluid depth increases. The base shear of the CV with the empty tank acts as an upper bound for the base shear of the fixed base CV with linear fluid and rigid fluid models. As with isolation displacement, mean peak base shear for the base isolated CV is not bound by the empty tank or rigid tank models. As a result, FSI should be accounted for when it is expected that the first asymmetric sloshing period may approach the isolation period.

## 5. CONCLUSIONS

This study presents an investigation into the effects of FSI in a base isolated NPP with an annular passive cooling tank, which is a common feature of Generation III+ NPP, using a fixed base NPP for reference. First, the predictions of a linear fluid sloshing model consisting of four asymmetric sloshing modes were compared against a nonlinear fluid model consisting of 16 sloshing modes under a moderate seismic hazard level. Sloshing height, lateral tank force, CV floor acceleration and CV floor displacement were compared for fixed base and base isolated CV with the following conclusions:

1. For NPP with annular passive cooling tanks of similar geometry to that studied, the linear fluid model consistently underestimates mean peak sloshing height. As such, it is not suitable for use in estimating sloshing height. A nonlinear fluid model should be used to design the required amount of freeboard for the tank. In situations where the excitation magnitude makes the nonlinear fluid model unusable, a more robust fluid model such as CFD model would be required.
2. The mean peak tank force predicted by the linear fluid model was in good agreement with predictions from the nonlinear fluid model for both the fixed base and base isolated NPP. By extension, the mean peak floor accelerations and mean peak floor displacements of the NPP were also in good agreement. Structural responses were estimated well enough by the linear fluid model

to warrant its use in the preliminary analysis of fixed base and base isolated NPP.

The linear model was then used to investigate the effect of FSI on fixed base and base isolated NPP with varying fluid heights. A linear fluid model at four discrete fluid depths, an empty tank, and a rigid fluid model were used to contrast how FSI affects the structural response of a base isolated NPP compared to a fixed base NPP with the following conclusions:

3. The rigid fluid model provided an upper bound on tank force for the fixed base NPP but not for the base isolated NPP. Thus, even though the tank force is reduced by introducing isolation, FSI should be accounted for in base isolated NPP design.
4. Floor response spectra for the fixed base NPP with the linear fluid model were enveloped by the spectra of the NPP with empty tank and rigid fluid models. As such, forces for non-structural components in fixed base NPP can be designed without explicit consideration of FSI. However, the floor spectra in the base isolated NPP were not enveloped by the empty tank and rigid fluid model spectra at periods exceeding 3s. Since most non-structural components have significantly shorter periods than 3s, their design can be conducted using the spectra without explicit consideration of FSI.

5. The mean peak displacement of base isolated and fixed base NPP with linear fluid models is bound by the empty tank and rigid fluid model cases. As such, an upper and lower bound for peak displacement of the NPP can be computed using two models that do not explicitly consider FSI.
6. The peak isolation displacement increases as the fundamental asymmetric sloshing mode period approaches the isolation period. This increase is dependent on the frequency content of the ground motion and is typically not bound by the results of empty and rigid fluid tank models. As such, FSI should be considered when performing analysis to determine the displacement capacity of the isolation system, as not considering FSI can significantly underestimate the peak displacement demands of the isolation system.



## 6. RECOMMENDATIONS FOR FUTURE WORK

### 6.1 LUMPED MASS-STICK MODEL

The representative lumped mass stick NPP model used in this study is a modified version of the lumped mass stick models used in Huang et al. (2008). The versions used in prior studies are three-dimensional, with masses attached with rigid links at eccentricities for the IS but not the CV. This is done to simulate torsion demands to the IS. The CV and IS models used in this study are in-plane and only the responses of the CV, which the tank is a part of, are examined in this study. This provides a good starting point to observe the effects of FSI on base isolated NPPs. Further research should investigate the effects of FSI on a three-dimensional finite element base isolated NPP to determine if the mass distribution and geometric simplifications inherent in lumped mass stick models notably effect the observations.

### 6.2 ISOLATION MODEL

The isolation design in this study uses a single FP isolation system for each site. This involved specifying a radius of curvature, a coefficient of friction and a displacement stop distance suitable for the seismic hazard at each site. In reality, it is likely that several FP isolation system designs would be developed and analyzed to determine the optimal design in terms of performance and cost for each location. A future research project could run a similar analysis and vary the coefficient of

friction and radius of curvature to investigate if an obvious combination exists that optimizes reduction in demand to the NPP. Furthermore, it could be examined that if the increase in isolation displacement associated with the design coefficient of friction of 0.02 is consistent at higher coefficients of friction, as increasing the coefficient of friction of an FP isolator typically decreases peak isolation displacement, all else being equal. Moreover, FPS isolators are not the only isolation system permitted for use in NPPs. A parallel analysis conducted for an NPP isolated using an LRB isolation system would provide insight to whether the performance of the isolation systems is comparable across two levels of seismic hazard, or if one is consistently better than the other.

### 6.3 FLUID TANK MODEL

The passive cooling tank of the representative NPP used in this study was idealized from an annular tank with sloped walls as an annular tank with straight walls. Liquid free surface and volume were kept constant for the idealization, however this meant that idealized tank's outer radius and fluid height changed when only the fluid height was altered for the actual tank. This makes it difficult to draw conclusions based solely on fill level, as the tank aspect ratio is significantly altered with changes in fluid height. More broad conclusions could be drawn if future work used an NPP with a passive cooling tank with constant cross section up its height, as this would limit the change in aspect ratio with fluid height. This could lead to an

investigation that determines if there is a limiting fluid to structure mass ratio at which the peak displacement of the isolation system is less affected by FSI.

## 7. REFERENCES

- Abali, E., & Uckan, E. (2010). Parametric analysis of liquid storage tanks base isolated by curved surface sliding bearings. *Soil Dynamics and Earthquake Engineering*, 30(1-2), 21–31. <https://doi.org/10.1016/j.soildyn.2009.08.001>
- Bandyopadhyay, K., Cornell, A., Costantino, C., Kennedy, R., Miller, C., & Veletsos, A. (1995). *Seismic Design and Evaluation Guidelines for The Department of Energy High-Level Waste Storage Tanks and Appertenances (BNL-52361)*. doi:10.2172/146793.
- Chen, J., Zhao, C., Xu, Q., & Yuan, C. (2014). Seismic analysis and evaluation of the base isolation system in AP1000 NI under SSE loading. *Nuclear Engineering and Design*, 278, 117–133. <https://doi.org/10.1016/j.nucengdes.2014.07.030>
- Christovasilis, I. P., & Whittaker, A. S. (2008). Seismic Analysis of Conventional and Isolated LNG Tanks Using Mechanical Analogs. *Earthquake Spectra*, 24(3), 599–616. <https://doi.org/10.1193/1.2945293>
- Faltinsen, O. M., Lukovsky, I. A., & Timokha, A. N. (2016). Resonant sloshing in an upright annular tank. *Journal of Fluid Mechanics*, 804, 608–645. <https://doi.org/10.1017/jfm.2016.539>
- Huang, Y.-N., Whittaker, A. S., Constantinou, M. C., & Malushte, S. (2007). Seismic demands on secondary systems in base-isolated nuclear power plants. *Earthquake Engineering and Structural Dynamics*, 36(12), 1741–1761. <https://doi.org/10.1002/eqe.716>
- Huang, Y.-N., Whittaker, A. S., & Luco, N. (2008). *Performance Assessment of Conventional and Base-Isolated Nuclear Power Plants for Earthquake and Blast Loadings (MCEER-08-0019)*. University at Buffalo, NY.
- Huang, Y.-N., Whittaker, A. S., & Luco, N. (2010). Seismic performance assessment of base-isolated safety-related nuclear structures. *Earthquake Engineering and Structural Dynamics*, 39(13), 1421–1442. <https://doi.org/10.1002/eqe1038>
- Ibrahim, R. (2005). *Liquid Sloshing Dynamics - Theory and Applications*. New York, NY: Cambridge University Press.
- Jaiswal, O.R., Durgesh, C.R., & Jain, S.K. (2007). Review of Seismic codes on Liquid-Containing Tanks.

- Earthquake Spectra, 23(1), 239–260. <https://doi.org/10.1193/1.2428341>
- Kammerer, A. M., Whittaker, A. S., & Constantinou, M. C. (2019). Technical Considerations for Seismic Isolation of Nuclear Facilities (NUREG/CR-7253). Retrieved from <https://www.nrc.gov/reading-rm/doc-collections/nuregs/contract/>
- Koh, J. M. (n.d.). Linear Harmonic Oscillator. Retrieved from <https://www.exoruskoh.me/linear-harmonic-oscillator>
- Kumar, M., Whittaker, A. S., & Constantinou, M. C. (2019). Seismic Isolation of Nuclear Power Plants Using Sliding Bearings (NUREG/CR-7254). Retrieved from <https://www.nrc.gov/reading-rm/doc-collections/nuregs/contract/>
- Kumar, M., Whittaker, A. S., & Constantinou, M. C. (2017). Extreme earthquake response of nuclear power plants isolated using sliding bearings. *Nuclear Engineering and Design*, 316, 9–25. <https://doi.org/10.1016/j.nucengdes.2017.02.030>
- Love, J. S., & Tait, M. J. (2015). The response of structures equipped with tuned liquid dampers of complex geometry. *Journal of Vibration and Control*, 21(6), 1171-1187. <https://doi.org/10.1177/1077546313495074>
- McNamara, K., Love, J. S., Tait, M. J., & Haskett, T. (2019, September). Annular tuned sloshing dampers for axisymmetric towers. The 15th International Conference on Wind Engineering, Beijing, China.
- Meserole, J. S., & Fortini, A. (1987). Slosh Dynamics in a Toroidal Tank. *Journal of Spacecraft and Rockets*, 24(6), 523–531.
- Moslemi, M., & Kianoush, M. R. (2016). Application of seismic isolation technique to partially filled conical elevated tanks. *Engineering Structures*, 127, 663–675. <https://doi.org/10.1016/j.engstruct.2016.09.009>
- National Institute of Standards and Technology (NIST) (2011). Selecting and scaling earthquake ground motions for performing response-history analyses (NIST GCR 11-917-15). Gaithersburg, MD.
- Paolacci, F. (2015). On the Effectiveness of Two Isolation Systems for the Seismic Protection of Elevated Tanks. *Journal of Pressure Vessel Technology*, 137(3), 031801. <https://doi.org/10.1115/1.4029590>

- Roberts, J. R., Basurto, E. R., & Chen, P.-Y. (1966). *Slosh Design Handbook I* (NASA CR-406). National Aeronautics and Space Administration, Washington, D.C.
- Saha, S. K., Matsagar, V. A., & Jain, A. K. (2014). Earthquake Response of Base-Isolated Liquid Storage Tanks for Different Isolator Models. *Journal of Earthquake and Tsunami*, 8(5), 1450013. <https://doi.org/10.1142/S1793431114500134>
- Seleemah, A. A., & El-sharkawy, M. (2011). Seismic response of base isolated liquid storage ground tanks. *Ain Shams Engineering Journal*, 2(1), 33–42. <https://doi.org/10.1016/j.asej.2011.05.001>
- Shivakumar, P., Veletsos, A., & Bandyopadhyay, K. (1994). Dynamic Response of Rigid Tanks with Inhomogeneous Liquids (BNL-52420). doi:10.2172/10154147.
- Shrimali, M. K., & Jangid, R. S. (2002). Non-linear seismic response of base-isolated liquid storage tanks to bi-directional excitation. *Nuclear Engineering and Design*, 217(1-2), 1–20. [https://doi.org/10.1016/S0029-5493\(02\)00134-6](https://doi.org/10.1016/S0029-5493(02)00134-6)
- Shrimali, M. K., & Jangid, R. S. (2003). Earthquake response of isolated elevated liquid storage steel tanks. *Journal of Construction Steel Research*, 59(10), 1267–1288. [https://doi.org/10.1016/S0143-974X\(03\)00066-X](https://doi.org/10.1016/S0143-974X(03)00066-X)
- Song, C., Li, X., Zhou, G., & Wei, C. (2017). Research on FSI effect and simplified method of PCS water tank of nuclear island building under earthquake. *Progress in Nuclear Energy*, 100, 48–59. <https://doi.org/10.1016/j.pnucene.2017.05.025>
- Sviatoslavsky, G., Prakash, A., Demitz, J., Vieira, A., & Reifschneider, M. (2013, August). *Sloshing in a Large Water Tank of a Non-standard Configuration Subjected to Seismic Loading*. 22nd Conference on Structural Mechanics in Reactor Technology. San Francisco, CA.
- Whittaker, A. S., Sollogoub, P., & Kim, M. K. (2018). Seismic isolation of nuclear power plants : Past , present and future. *Nuclear Engineering and Design*, 338, 290–299. <https://doi.org/10.1016/j.nucengdes.2018.07.025>
- Xu, Q., Chen, J., Zhang, C., Li, J., & Zhao, C. (2016). Dynamic Analysis of AP1000 Shield Building Considering Fluid and Structure Interaction Effects. *Nuclear Engineering and Technology*, 48(1), 246–258. <https://doi.org/10.1016/j.net.2015.08.013>

- Zhao, C., Chen, J., & Xu, Q. (2014). FSI effects and seismic performance evaluation of water storage tank of AP1000 subjected to earthquake loading. *Nuclear Engineering and Design*, 280, 372–388. <https://doi.org/10.1016/j.nucengdes.2014.08.024>
- Zhao, C., & Yu, N. (2018). Dynamic response of generation III + integral nuclear island structure considering fluid structure interaction effects. *Annals of Nuclear Energy*, 112, 189–207. <https://doi.org/10.1016/j.anucene.2017.10.011>

## APPENDIX A

Table A. Ground motions used in Diablo Canyon Analysis (10,000-year return period).

GM Number	PEER RSN	Event	Scale Factor	Magnitude	Rupture Distance (km)
1	77	San Fernando	1.3	6.6	1.8
2	143	Tabas	1.0	7.4	2.1
3	184	Imperial Valley	2.5	6.5	5.1
4	285	Irpinia	5.0	6.9	8.2
5	802	Loma Prieta	2.6	6.9	8.5
6	1633	Manjil	2.2	7.4	12.6
7	179	Imperial Valley	2.7	6.5	7.1
8	1107	Kobe	5.5	6.9	22.5
9	1787	Hector Mine	4.3	7.1	11.7
10	183	Imperial Valley	2.5	6.5	3.9
11	985	Northridge	4.4	6.7	29.9
12	1521	Chi-Chi	2.9	7.6	9.0
13	549	Chalfant Valley	5.6	6.2	17.2
14	755	Loma Prieta	5.5	6.9	20.3
15	1209	Chi-Chi	5.2	7.6	24.1

Table B. Ground motions used in Vogtle Analysis (2475-year return period).

GM Number	PEER RSN	Event	Scale Factor	Magnitude	Rupture Distance (km)
1	882	Landers	0.99	7.3	26.8
2	1100	Kobe	0.81	6.9	24.8
3	184	Imperial Valley	0.32	6.5	5.1
4	284	Irpinia	2.53	6.9	9.6
5	285	Irpinia	0.65	6.9	8.2
6	802	Loma Prieta	0.33	6.9	8.5
7	1633	Manjil	0.29	7.4	12.6
8	179	Imperial Valley	0.35	6.5	7.1
9	754	Loma Prieta	0.99	6.9	20.8
10	1107	Kobe	0.71	6.9	22.5
11	1787	Hector Mine	0.55	7.1	11.7
12	183	Imperial Valley	0.33	6.5	3.9
13	985	Northridge	0.57	6.7	29.9
14	1521	Chi-Chi	0.37	7.6	9.0
15	3302	Chi-Chi	1.05	6.3	70.4